Original Research Article

Green-Synthesized Ag/TiO_2 Nanocomposite Photoanodes Using *Glyricidia* sepium Extract for Enhanced Charge Transport in Dye-Sensitized Solar Cells

Joseph Adegbite Adebanji[1], Gabriel Ayinde Alamu[1,*], Olufunke Lydia Adedeji[2], Khadijat Kuburat Babalola[3], Ayodele Joshua Abiodun[4], Hakeem Olayinka Oyeshola[1], Oluwaseun Adedokun[1,5,*], Yekinni Kolawole Sanusi[1,5]

[1]*Department of Pure and Applied Physics, Ladoke Akintola University of Technology, Ogbomoso, Nigeria*
[2]*Department of Chemical Science, Yaba College of Technology, Yaba, Nigeria*
[3]*Department of Physical and Chemical Sciences, Federal University of Health Sciences, Ila-Orangun, Nigeria*
[4]*Department of Physics, Lead City University, Ibadan, Oyo, Nigeria*
[5]*Nanotechnology Research Group (NANO+), Ladoke Akintola University of Technology, Ogbomoso, Nigeria*

Citation J.Adegbite. Adebanji, G.A. Alamu, O.L. Adedeji, K.K. Babalola, A.J. Abiodun, H.O. Oyeshola, O. Adedokun, Y.K. Sanusi. Green-Synthesized Ag/TiO_2 Nanocomposite Photoanodes Using *Glyricidia* sepium Extract for Enhanced Charge Transport in Dye-Sensitized Solar Cells. *J. Eng. Ind. Res.* **2026**, 7 (1):29-47.
https://doi.org/10.48309/JEIRES.2026.536373.1293

Article info:
Submitted: 2025-08-02
Revised: 2025-08-29
Accepted: 2025-09-16
ID: JEIRES-2508-1293

Keywords:
Nanostructured photoanode; Enhanced electrical conductivity; Ag/TiO_2 nanocomposite; Dye-sensitized solar cell; *Gliricidia septum*.

ABSTRACT

This study effectively demonstrated the use of *Gliricidia sepium* (*G. sepium*) leaf extract in the formation and characterization of a green-synthesized silver/titanium dioxide (Ag/TiO_2) nanocomposite, as well as its use as an enhanced photoanode material in dye-sensitized solar cells (DSSCs). The production of the silver nanoparticles (AgNPs) was established by UV-Vi's spectra of the plasmon resonance band, which was detected at around 420 nm. Due to the incorporation of the nanoparticles with TiO_2, the energy gap clearly decreased. The functional groups and their probable contribution to the formation of the nanoparticles and nanocomposite were identified by Fourier Transform Infrared (FTIR) investigations. X-ray Diffraction (XRD) studies revealed that the produced nanoparticles and nanocomposite had average crystallite sizes of 3.69 nm and 4.04 nm, respectively. Spherical, smoother, and more uniform particles were visible in the synthesized nanocomposite's Scanning Electron Microscopy (SEM) image. The TiO_2 nanocomposite's Energy Dispersive Spectra (EDS) confirmed the existence of Ag and other constituent elements. The creation of nanoparticles and nanocomposite with average particle sizes of 4.14 nm and 5.39 nm was further confirmed by the evaluation of the particles' Transmission Electron Microscopy (TEM) micrographs. The conductivity of the TiO_2 photoanode was improved by 73.11% after the inclusion of the AgNPs, leading to promising electrical characteristics that indicate its suitability in DSSCs.

***Corresponding Author: Oluwaseun Adedokun** (oadedokun@lautech.edu.ng); **Gabriel Ayinde Alamu** (gaalamu19@lautech.edu.ng)*

Introduction

Dye-sensitized solar cells (DSSCs), a promising photovoltaic technology, are affordable, simple to fabricate, and have an extensive range of potential uses. The material used for the photoanode, typically made of a semiconductor material such as titanium dioxide (TiO_2), has a considerable impact on the performance of DSSCs. The excellent stability, non-toxicity, and appropriate electrical characteristics of TiO_2 make it the ideal material for DSSC photoanodes. However, TiO_2's effectiveness in DSSCs is limited by its relatively low electrical conductivity. Increasing the TiO_2 photoanode's electrical conductivity can significantly enhance the overall performance of DSSCs [1,2]. One of the main objectives of improving the electrical conductivity of TiO_2 in DSSCs is to increase the photocurrent and total power conversion efficiency (PCE) of the device. The number of electrons that are successfully injected into TiO_2's conduction band and transferred to the external circuit is directly correlated with the photocurrent. A larger photocurrent results from more photogenerated electrons being able to be carried without recombining when TiO_2's electrical conductivity is increased. The PCE, which is influenced by the photocurrent, open-circuit voltage (Voc), and fill factor (FF), is commonly used to describe the efficiency of DSSCs. Through faster electron transport made possible by improved TiO_2 conductivity, the photocurrent can be increased, raising the cell's overall PCE. Numerous studies have shown that TiO_2 can be modified to enhance its conductivity, which, in turn will result in increased photocurrent and PCE. Examples of these modifications include doping with other elements or employing TiO_2 composites [3,4].

Improving the electrical conductivity of TiO_2 in DSSCs has the most immediate and important advantage of increasing charge transport efficiency. Enhancing TiO_2's electrical conductivity makes electron transport quicker and more effective, facilitating the migration of electrons to migrate from the dye to the conductive substrate. Because fewer recombination events occur as a result of the decreased electron transport resistance, more photogenerated electrons are efficiently captured by the electrode, increasing the production of current and power. Because the photoanode can swiftly and efficiently gather and transfer electrons to the external circuit, improved charge transport also enables the DSSC to function even more effectively in low light conditions [5]. For DSSCs to be practically used in solar energy applications, their long-term stability is essential. The tendency of the TiO_2 photoanode to develop flaws over time, particularly when exposed to light and environmental factors for extended periods of time, is one of its primary problems. These flaws have the potential to raise electron recombination rates and lower the cell's overall efficiency. The overall stability of the DSSC can be augmented by increasing the electrical conductivity of TiO_2. This is because, over time, a higher conductivity results in fewer defects and lower recombination rates since it lowers the energy barriers for electron transport. Additionally, the improved charge transport properties lessen the cell's vulnerability to degradation caused by charge accumulation at interfaces, which over time can degrade materials and lower the device's efficiency. Furthermore, increasing TiO_2's conductivity can strengthen its defenses against environmental elements, including heat, moisture, and UV rays. As a result, the DSSC's operational lifetime increases, enhancing its dependability and durability for practical uses. The stability of the cell under varied climatic circumstances is enhanced by materials with higher conductivity,

which are generally better equipped to withstand the stresses and strains of prolonged use [6]. Another important factor that affects a DSSC's effectiveness is its series resistance (Rs). A high Rs lowers the device's overall performance by limiting the amount of current that can pass through it. The resistive characteristics of the photoanode, the electrolyte, and the external circuit are some of the sources of the Rs. Due to TiO_2's comparatively low electrical conductivity, a sizable amount of the Rs in DSSCs using it as the photoanode stems from this material. The FF of the device can be improved significantly by lowering the Rs through increasing the electrical conductivity of TiO_2. A higher FF indicates a more efficient solar cell. The FF is a measurement of the maximum power output from a solar cell in relation to its theoretical maximum power. A greater FF is made possible by the TiO_2 photoanode's enhanced conductivity, which lowers resistance to the electron flow and raises the overall performance of the DSSC's PCE [7,8]. While electron transport is the main function of TiO_2 in DSSCs, the material also contributes to light absorption and scattering, especially in mesoporous TiO_2 photoanodes. Enhancing TiO_2's electrical conductivity can also boost its capacity to capture light. This is due to the fact that conductivity boosting alterations (such doping or the inclusion of conductive carbon-based materials) can affect the shape and porosity of the TiO_2 film, improving light scattering within the photoanode. The probability that incident photons will interact with the dye molecules is increased by improved light scattering, which results in more effective electron excitation and injection into the TiO_2 conduction band. This enhances the DSSC's total light absorption capabilities, increasing the device's capacity to capture sunlight, especially in diffuse light. Even in less-than-ideal illumination conditions, the DSSC can function more effectively by enhancing TiO_2's electrical conductivity and light-harvesting capacities [9].

The possibility of more effective and economically feasible DSSCs grows as research into other techniques to improve TiO_2 conductivity, such as doping, composite creation, and surface modifications, progresses. Therefore, improving TiO_2's electrical conductivity is essential for creating high-performance DSSCs that can rival conventional silicon-based solar cells. The addition of silver nanoparticles (AgNPs) to TiO_2 photoanode is one such improvement. AgNPs have distinct optical, electrical, and catalytic qualities, and it has been demonstrated that integrating them into the TiO_2 matrix enhances DSSC performance in several ways. The enhancement of light absorption and scattering characteristics is one of the main benefits of adding AgNPs to TiO_2 photoanodes. Conduction electrons on the surface of AgNPs vibrate in response to incident light, a process known as surface plasmon resonance (SPR), which increases light absorption in the visible spectrum. This extends the path length of light within the TiO_2 layer, ultimately increasing the number of photons that the dye molecules on the photoanode surface can absorb. Additionally, adding AgNPs to TiO_2 can enhance the photoanode's electron transport capabilities. By facilitating the creation of conductive pathways for electrons, the AgNPs can improve electron mobility and lower the resistance to charge transport. In addition to being efficient electron sinks, AgNPs also capture and move electrons produced by dye molecules to the external circuit. Moreover, AgNPs have the ability to reduce the I^{3-} ion in the electrolyte by acting as a catalyst. Higher photocurrents and better cell performance result from this process, which also reduces electron recombination losses and improves the DSSC's overall charge transport dynamics [10].

One aspect of sustainable nanotechnology, which employs natural resources to create

nanoparticles in a way that minimizes waste and contamination, is the synthesis of AgNPs using plant-based materials.

The production of AgNPs from plant leaves has the potential to be a renewable and sustainable resource that promotes environmental preservation. Furthermore, it is relatively inexpensive to synthesize AgNPs using plant extracts since plant leaves are readily available, easy to collect, and do not require costly chemicals, making them a low-cost alternative to large-scale AgNP production. The green synthesis of AgNPs is a straightforward procedure that does not require many steps, aside from the availability of raw materials. The technique's simplicity makes it affordable and suitable for resource-constrained situations where access to more sophisticated chemical procedures may be restricted. Two significant advantages of producing AgNPs from plant leaves are their biocompatibility and low toxicity. The green synthesis method employs plant extracts that contain phytochemicals such as flavonoids, alkaloids, and polyphenolic compounds, as opposed to those made using conventional chemical procedures. By stabilizing AgNPs, these phytochemicals lessen their detrimental effects on living organisms [11]. For instance, neem (*Azadirachta indica*) leaf has been extensively researched for the environmentally friendly production of AgNPs. In a study, AgNPs were created by Verma Mohan and Mehata (2015) using silver salt and an aqueous extract of neem leaves. Measurements and analyses were conducted using XRD, SEM, FTIR, optical absorption, and photoluminescence (PL). Based on the results, the plant-based resources can be effectively exploited to produce AgNPs, which may find applications in a variety of sectors, including nanotechnology and biomedicine [12]. In another study, Alamu *et al.* (2021) used henna (*Lawsonia inermis*) leaf extract to evaluate the impact of plasmonic green-synthesized AgNPs dispersed in TiO_2 on the overall performance of DSSC. The results demonstrated that plasmonic green-synthesized AgNPs integrated with TiO_2 as the photoanode material and natural dyes as sensitizers are excellent materials for the production of DSSCs with exceptional environmental friendliness [1].

Recently, *G. sepium* plant came into limelight and it was discovered that its extract contains very rich phytochemicals that could be used for the synthesis of nanoparticles which could find applications in various sectors. For instance, Raut *et al.* (2009) examined the use of *G. sepium* (also called Glyricidia or quick stick) leaves for the green synthesis of AgNPs. The plant was found to contain a rich content of bioactive compounds, including flavonoids, phenolic acids, terpenoids, and alkaloids, which acted as both stabilizing agents and reducing agents for the AgNPs, making the synthesis process sustainable and environmentally friendly. The phytosynthesis method seemed to be an accessible, affordable, and environmentally acceptable substitute for traditional AgNP synthesis techniques. The reduced average size of the particles, as demonstrated through TEM analysis, proved that the extract from the plant is useful for the synthesis of nanoparticles that could be used to modify TiO_2 photoanode of DSSCs [13].

Evidently, researchers have shown that the surface area of AgNPs increases as their particle size decreases. Collisions are more likely as a result, and reaction times quicken [14]. The shape and size of AgNPs affect their characteristics, and the type and concentration of phytochemicals in the plant determine the desirable form and reactivity of AgNPs made from plant resources [15]. A greater surface area is needed to enhance the electrical conductivity and light absorption of TiO_2, and the surface area is related to the nanoparticle size [16]. Researchers have shown in different fields of study that the extract of Gliricidia leaf is rich in

phytochemicals that could be used for the synthesis of AgNPs with large surface area, but its potential has not yet explored in DSSC photoanodes.

Thus, to improve the electrical conductivity in DSSCs, this study examined the application of *G. sepium* leaf extract in the synthesis and characterization of a green-synthesized Ag/TiO_2 nanostructured photoanode. The characterizations were carried using UV–Vi's spectroscopy, FTIR, XRD, SEM, EDS, and TEM analyses. The four-point probe technique was employed to electrically characterize the TiO_2 and modified TiO_2 films.

Experimental

Materials

Without further purification, Sigma-Aldrich's silver nitrate ($AgNO_3$) salt and TiO_2 powder (P25) were used. The Forestry Research Institute of Nigeria (FRIN) in Jericho, Ibadan, provided the fresh *G. sepium* leaves. We purchased non-conductive glass slides from XIN Yan Technology Limited in China.

Green synthesis of AgNPs

The gathered fresh *G. sepium* leaves are displayed in Figure 1(a). After washing the leaves with distilled water, they were allowed to air dry. The leaves were then crushed into powder before being stored. The powder (20 g) that was weighed was boiled with deionized water (1 liter) for 30 minutes at 60 °C, and its extract was then filtered through Whatman No. 1 filter paper [1]. Distilled water (100 ml) was mixed with $AgNO_3$ (0.017 g) to make a solution (1 mM) of $AgNO_3$. After that, each extract (2 ml to 10 ml at intervals of 2 ml) was added separately to the solution (10 ml of 1 mM $AgNO_3$) to produce AgNPs, maximizing the volume of the extract needed for AgNP production. The reason the samples were varied for AgNP production is shown in Figure 1(b).

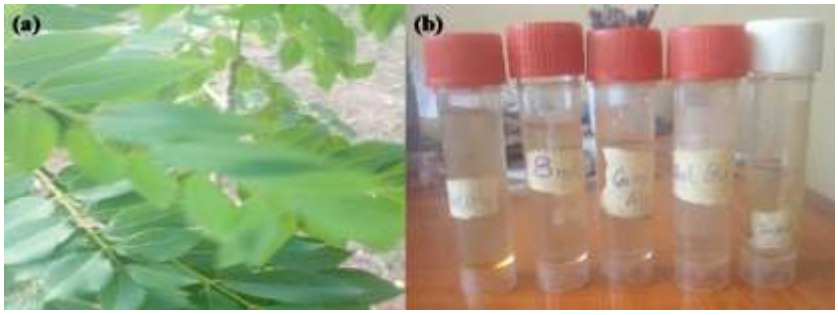

Figure 1: (a) *G. sepium* leaves (b) AgNPs at different volumes of *G. sepium* leaves extract

Figure 2: Deposited films

Deposition of films

TiO_2 powder (1.5 g) was placed in a sterile beaker. Distilled water (2.5 ml) was added to the aggregates to break them up into individual particles. Ethyl cellulose (0.5 g) was dissolved in 50 ml of ethanol and added to the sample. Following the addition of 5 ml of terpeneol, the mixture was placed on the magnetic stirrer. The mixture was heated to 60 °C, and 50 ml of ethanol was added at regular intervals under continuous stirring for 1 hour to create a homogeneous paste. Various volume fractions of the optimized AgNPs for film fabrication (0.5 ml, 1.0 ml, 1.5 ml, and 2.0 ml) were mixed with the paste (1 ml) to further optimize the volume required for an enhanced photoanode in DSSC. After being cleaned with a detergent solution, the glass substrates were ultrasonically cleaned for 15 minutes at 30 ^oC. After that, the substrates were also cleaned with isopropanol alcohol (IPA) for 30 minutes at 30 ^oC. Initially, the glass substrates were wrapped with adhesive tape on two corresponding edges to control the film regions and provide uncoated spaces for electrical measurements. The resulting pastes were placed at one edge of the cleaned glass substrates and then spread out using a glass rod. Additionally, a reference electrode free of nanoparticles was created. The films were dried at 125 ^oC for 15 minutes after being allowed to relax for a few minutes to reduce surface defects. After that, the optical, and electrical characterizations were carried out [17]. Figure 2 shows the film samples that were applied to the glass substrates.

Characterizations

The UV-Vis spectrometer (ASUV-6300PC for the nanoparticles and Avantes model Avalight DH 5 BAL for the thin films) was used to analyze the optical absorptions, while the NICOLET iS10 spectrometer was used to analyze the FTIR spectrophotometry. The XRD and morphology of the films were characterized using a Rigaku D/Max-IIIC XRD instrument and a scanning electron microscope (JOEL-JSM 7600F). JEM-ARM200F-G TEM equipment was used to conduct TEM investigation to examine the sizes and shapes of the nanoparticles, TiO_2, and modified TiO_2. A four-point probe (KEITHLEY instrument, 6220 DC current source) was used to measure the electrical characteristics.

Results and discussion

Optical studies

Optical absorbance of the AgNPs

The samples were optically characterized in order to verify the optimal amount of leaf extract to mix with $AgNO_3$ to form AgNPs. Figure 3 displays the UV-Vis optical absorptions of the AgNPs produced with varying volumes of the leaf extract as a reducing agent. The activation of surface plasmon vibrations in AgNPs caused the color to gradually change from brown to yellowish brown as the leaf extract and the $AgNO_3$ aqueous solution were combined [18]. The synthesis of AgNPs was validated by the production of strong yellowish-brown solutions. The plasmon resonance band's UV spectra at around 420 nm are comparable to those found in previous research. The intensity of absorption decreased as the extract volume increased. Additionally, the SPR band of AgNPs redshifted as the volume of leaf extract increased. This implies that a small amount of the extract was required in order for the AgNPs to form [19]. Visual inspection also showed that the AgNPs formed quickly within a few minutes. Only 2 ml of the extract was essential for the nanoparticle formation, as evidenced by the absorbance spectrum, with 2 ml of the extract showing the greatest peak at about 420 nm. As a result, 2 ml of the extract combined with 10 ml of a 1 mM $AgNO_3$ solution produced a well-synthesized

AgNPs. Later, the AgNPs containing 2 ml of the extract were utilized to fabricate the films.

Optical absorbance of TiO_2 films with AgNPs

Figure 4 displays the UV-Vis optical absorption of the film samples with and without AgNPs made from the leaf extract of *G. sepium*. Due to a wide band gap, the sample without AgNPs did not exhibit any absorbance in the visible spectrum. Because of the AgNPs' SPR band, combining them with TiO_2 paste affected their absorbance in the visible spectrum. It has been shown that SPR in AgNPs improves charge generation in DSSCs and increases light trapping. It is a method that shows promise for improving DSSC performance [1]. The sample containing 2 ml of the AgNPs exhibited the maximum absorption. Consequently, it was applied to further characterization.

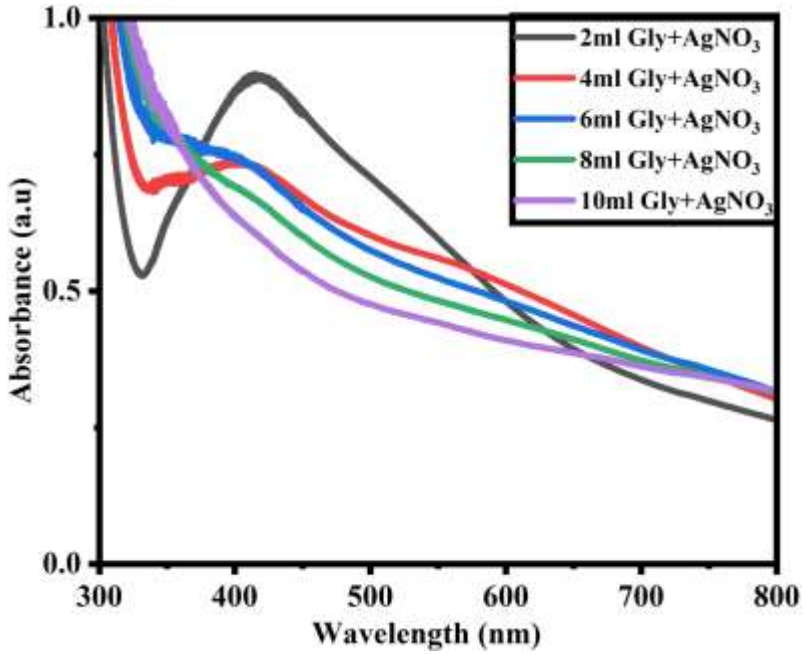

Figure 3: Optical absorbance of AgNPs synthesized with different volumes of *G. sepium* leaves extract

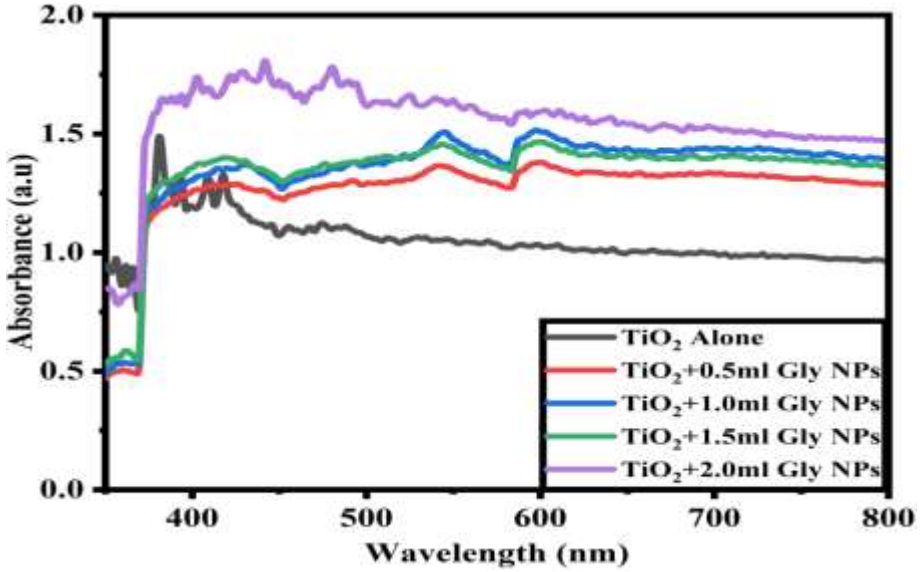

Figure 4: Optical absorbance of TiO_2 film samples incorporated with the AgNPs

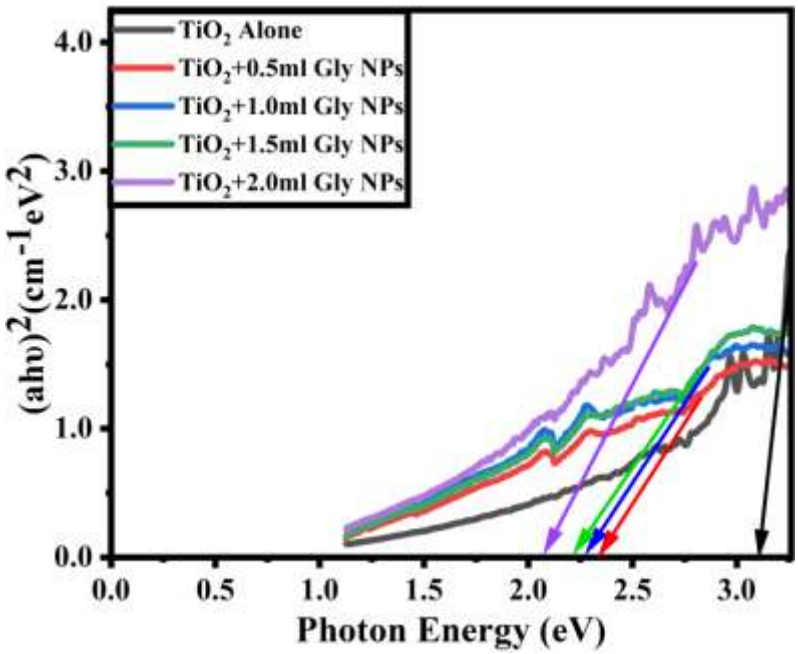

Figure 5: Optical band gap of the TiO_2 films incorporated with the AgNPs

Table 1: Optical band gap of the TiO_2 films incorporated with the AgNPs

Sample	Energy gap (eV)
TiO_2 sample alone	3.25
TiO_2 sample with 0.5 ml AgNPs	2.33
TiO_2 sample with 1.0 ml AgNPs	2.30
TiO_2 sample with 1.5 ml AgNPs	2.24
TiO_2 sample with 2.0 ml AgNPs	2.10

Optical band gaps of TiO_2 film samples

Figure 5 demonstrates the optical band gaps for the TiO_2 samples. As can be observed, the figure shows that as the volume of the AgNPs increased, the band gap reduced. Table 1 indicates the findings, which suggest that as absorbance rises, the energy gap falls. Since electrons will need less energy to move all the way through the material's Fermi level, a decrease in the energy gap indicates an increase in conductivity [20]. Since it results in more light absorption, a larger population of excited electrons, and more fruitful catalytic processes, decreasing the optical band gap in TiO_2 films is important for their photocatalytic behavior [21]. As a result, lowering the film's bandgap boosts electron transport to the TiO_2 conduction band, increasing the TiO_2 photoanode's effectiveness [20].

FTIR spectroscopy

FTIR spectroscopy of the AgNPs

FTIR spectral of the *G. sepium* leaf extract and the AgNPs are shown in Figure 6. The IR band detected at 699.20 cm^{-1} in the extract is attached to C-Br stretching of halo compound; 1,063.20

cm^{-1} to strong C-O stretching of primary alcohol; 1,619.60 cm^{-1} to the N-H bending vibration of the amine group; 2,364.80 cm^{-1} to strong O=C=O stretching of carbon dioxide; 2,760.80 cm^{-1} to medium C-H stretching of doublet aldehyde group; 3,277.67 cm^{-1} and 3,216.00 cm^{-1} to strong, broad O-H stretching of carboxylic acid and 3,921.80 cm^{-1} with 3780.80 cm^{-1} to medium, sharp O-H stretching of free alcohol [22,23].

Also, the band at 1,395.32 cm^{-1} belongs to medium O-H bending of carboxylic acid; 2,889.69 cm^{-1} to medium C-H stretching of alkane compound and 3,417.67 cm^{-1} to strong, broad O-H stretching of intermolecular bonded alcohol compound [23].

The transmittances in the AgNPs located at 665.60 cm^{-1} and 873.88 cm^{-1} represent the strong C=C bending of the disubstituted and vinylidene alkane compound, while the peak at 1,064.00 cm^{-1} belongs to the strong S=O stretching of the sulfoxide compound. Additionally, the peaks at 1,258.47 cm^{-1} and 1,326.63 cm^{-1} represent the strong C-O stretching of the aromatic ester compound which might be due to the existence of covalent linking of ether or ester groups with the AgNPs [24]. The band at 1,629.60 cm^{-1} belongs to medium C=C stretching of the disubstituted alkane compound; 1,946.87 cm^{-1} to weak C-H bending of overtone aromatic compound; 2,361.60 cm^{-1} to the strong O=C=O stretching of carbon dioxide; 2,760.00 cm^{-1}, 2,915.32 cm^{-1} and 3,123.40 cm^{-1} to weak, broad intramolecular bonded O-H stretching of alcohols; 3,302.42 cm^{-1} and 3,409.03 cm^{-1} to strong, broad intermolecular bonded O-H stretching of alcohols and 3,643.24 cm^{-1} with 3,819.03 cm^{-1} and 3,899.20 cm^{-1} to medium, sharp and free O-H stretching of alcohols. There are shifts in many of the IR bands; some disappeared completely, while new bands appeared which might be due to the possible contribution of the different functional groups to the formation of the AgNPs [25].

The existence of distinctive absorption bands of *G. sepium* leaf extract phytoconstituents in the AgNPs was discovered by comparing the infrared spectra of the two substances. These bands show that AgNPs bind to carboxylate groups of proteins and alcohol [25].

The diminution of the Ag salt to AgNPs and their stabilization, which led to the crystallization of the bio-organic phase on their surface, are thus attributed to the contribution of all these functional groups of *G. sepium* leaf extract. It is known that functional groups in biological components interact with metal salts to mediate the production of nanoparticles [26].

The potential functional groups that are responsible for the stabilization and reduction of the produced AgNPs were therefore determined by the FTIR data.

The FTIR absorption values of the extract and the AgNPs are shown in Table 2.

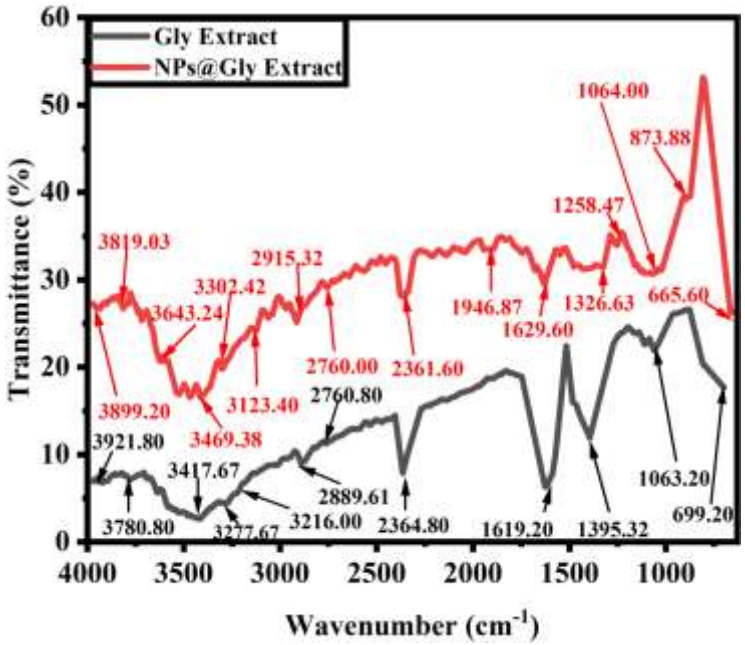

Figure 6: FTIR analysis of *G. sepium* leaf extract and the AgNPs

Table 2: The FTIR absorption values of the extract and the AgNPs

Wave number (cm^{-1})	*G. sepium* leaf extract	AgNPs @ *G. sepium* leaf extract	Functional group
4,000-3,000	3,922; 3,781; and 3,418, 3,278; 3,216	3,899; 3,819; 3,643; 3,409; 3,302; and 3,123	O-H (stretching)
3,000-2,500	2,889; 2761	2,915; 2,760	C-H (stretching)
2,400-2,000	2365	2,362	O=C=O (stretching)
2,000-1,650	-	-	C-H (bending)
1,650-1,600	1,619	1,630	C=C (stretching)
1,600-1,300	1,395	1,327	N-O (stretching)
1,300-1,000	1,063	1,064	O-H (bending)
1,000-650	699	665	C=C (bending)

FTIR spectroscopy of TiO_2 and Ag/TiO_2 nanocomposite

FTIR spectra of TiO_2 and modified TiO_2 are shown in Figure 7. The IR band detected at 608.09 cm^{-1} in the TiO_2 is attributed to C-Br stretching of halo compounds; 1,029.22 cm^{-1} to medium, C-N stretching of amines; 1,086.47 cm^{-1} to strong C-O stretching of aliphatic ethers; 1,311.74 cm^{-1} and 1,382.40 cm^{-1} to medium, O-H bending of phenols and 1,630.21 cm^{-1} to the strong, C=C stretching of monosubstituted alkene. Also, the band at 2,358.10 cm^{-1} belongs

to strong O=C=O stretching of carbon dioxide; 2,925.12 cm^{-1} to medium, C-H stretching of alkane groups; 3,419.79 cm^{-1} to strong, broad O-H stretching of intermolecularly bonded alcohols and 3,768.00 cm^{-1} to medium, sharp O-H stretching of free alcohols [22,23].

The IR band detected in the modified TiO_2 located at 1,032.00 cm^{-1} represents the strong S=O stretching of sulfoxide compounds, while the peak at 1,369.00 cm^{-1} represents the strong S=O stretching of the sulfonamide compounds [24].

The band at 1,595.00 cm^{-1} belongs to medium C=C stretching of the cyclic alkene compound; 2,360.17 cm^{-1} to the strong O=C=O stretching of carbon dioxide; 2,853.01 cm^{-1} to medium, C-H stretching of alkane compounds; 2,918.00 cm^{-1} signifies weak, broad intramolecular bonded O-H stretching of alcohols; and 3,778.31 cm^{-1} indicates medium, sharp and free O-H stretching of alcohols. There are also many shifts in the IR bands; some disappeared completely, while new bands appeared which might also be due to the possible interactions of the different functional groups in the nanoparticle with the TiO_2 [25]. The existence of distinctive absorption bands of the phytoconstituents of the AgNPs in the TiO_2 was discovered by comparing the infrared spectra of the two materials.

These bands show that the AgNPs bind to the carboxylate groups of proteins and alcohol [25]. Table 3 presents FTIR absorption values of the TiO_2 and modified TiO_2.

Table 3: The FTIR absorption values of the TiO_2 and Ag/TiO_2 nanocomposite

Wave number (cm^{-1})	TiO_2	Ag/TiO_2	Functional group
4,000-3,000	3,768.00; 3,419.79	3,778.31; 3,376.00	O-H (stretching)
3,000-2,500	2,925.12	2,918.00; 2853.01	C-H (stretching)
2,400-2,000	2,358.10	2,360.17	O=C=O (stretching)
2,000-1,650	-	-	C-H (bending)
1,650-1600	1,630.21	-	C=C (stretching)
1,600-1300	1,383.40; 1,311.74	1,595.00; 1369.00	N-O (stretching)
1,300-1000	1,086.47; 1029.22	1,032.00	O-H (bending)
1,000-650	608.09	-	C=C (bending)

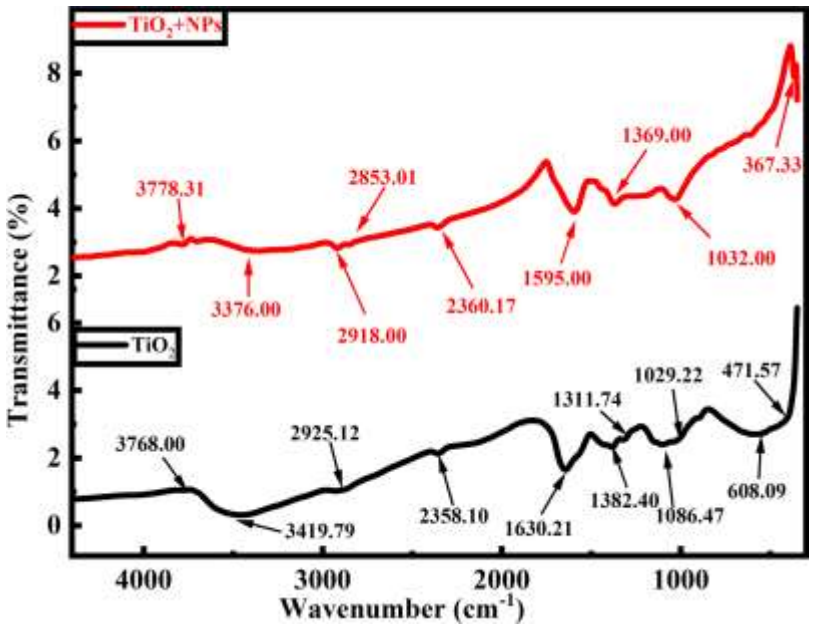

Figure 7: FTIR analysis of TiO_2 and Ag/TiO_2 nanocomposite

Structural studies of Ag/TiO_2 nanostructures

The XRD patterns of the AgNPs, TiO_2, and TiO_2 modified with the AgNPs were performed, so as to verify the phase development of the samples, as illustrated in Figure 8. The significant peaks and their corresponding planes are clearly visible in Figure 8(a). It was discovered that the pattern was crystalline and had a face-centered cubic (FCC) structure when the AgNPs index was formed using the JCPDS card (file no.: #030931) [27]. The average crystallite size of the AgNPs was determined to be 3.69 nm by applying Debye-Scherrer's equation [28]. It was clear from the stronger planes that silver played a significant role in the biosynthesis. Similar findings for AgNPs were reported by previous researchers [29].

According to Figure 8(b), the TiO_2 is composed of a mixture of rutile and anatase phases, which is consistent with the JCPDS reference pattern on card number #83-2243. It was discovered that the pattern was crystalline and had a body-centered tetragonal structure. The average crystallite size was estimated to be 7.47 nm.

The average crystallite size was 4.04 nm when the TiO_2 was added to the AgNPs. The modified sample is crystalline in nature with a face-centered cubic structure, as shown in Figure 8(c). This aligns well with the JCPDS reference pattern, card number #21-1276. The rutile phase of the TiO_2 and the AgNPs-induced peaks in the nanocomposite nearly coincide. As a result, the peaks in the TiO_2 nanocomposite are similar, demonstrating that AgNPs were successfully doped into the TiO_2. The sample's average crystallite size significantly decreased, indicating that the TiO_2 photoanode improved in efficiency and is effective for DSSC manufacturing [14].

The surface area per unit mass of AgNPs increases as the crystallite size decreases. Nanoparticles with a higher surface area-to-mass ratio are beneficial in DSSC applications because they can interact with their environment more effectively. Particles with nanometer-scale dimensions in quantum mechanics undergo special effects such as quantum confinement. These effects have the potential to change the electrical properties of AgNPs, which could result in enhanced catalytic

activity and optical behaviors [10]. The plasmonic resonance observed in AgNPs, which has applications in DSSC, is also influenced by quantum confinement. AgNPs' stability and dispersibility are also affected by their very small crystallite sizes. Ag particles in bulk materials can aggregate, which decreases their utility in applications requiring dispersion in a liquid or gas environment. AgNPs can be distributed more readily without aggregating by maintaining their crystallite sizes small, ensuring that their unique properties are preserved in a useful form. By providing additional active sites for chemical reactions, these particles can enhance reaction rates and efficiency in DSSC [10].

Morphological studies of Ag/TiO_2 nanostructures

Figure 9 displays the TiO_2 and TiO_2 incorporated with the synthesized AgNPs SEM micrographs. As seen in Figure 9(a), the TiO_2's SEM micrograph indicates a porous structure. As seen in Figure 9(b), the sample's surface features changed after the AgNPs were added, resulting in a more spherical shape. With no discernible areas of aggregated particles, the morphology became apparent, homogeneous, and dense [30].

The composition of titanium and oxygen in TiO_2 was verified by the EDS analysis, demonstrating that it was pure TiO_2. The existence of Ti, O and Ag is confirmed by the EDS results for the TiO_2 nanocomposite. The presence of the AgNPs was verified by the distinctive Ag peak that was observed.

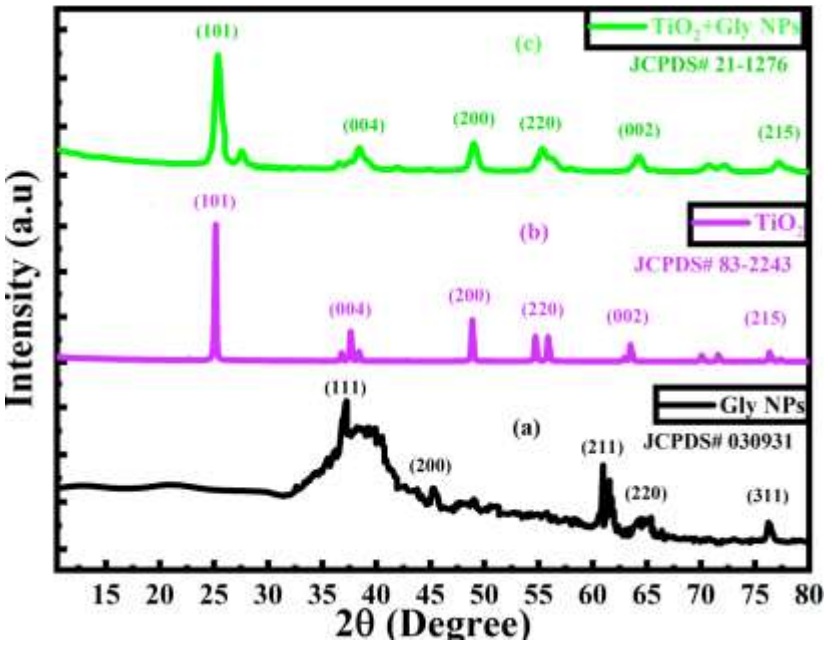

Figure 8: XRD patterns of (a) AgNPs, (b) TiO_2 alone, (c) TiO_2 incorporated with the AgNPs

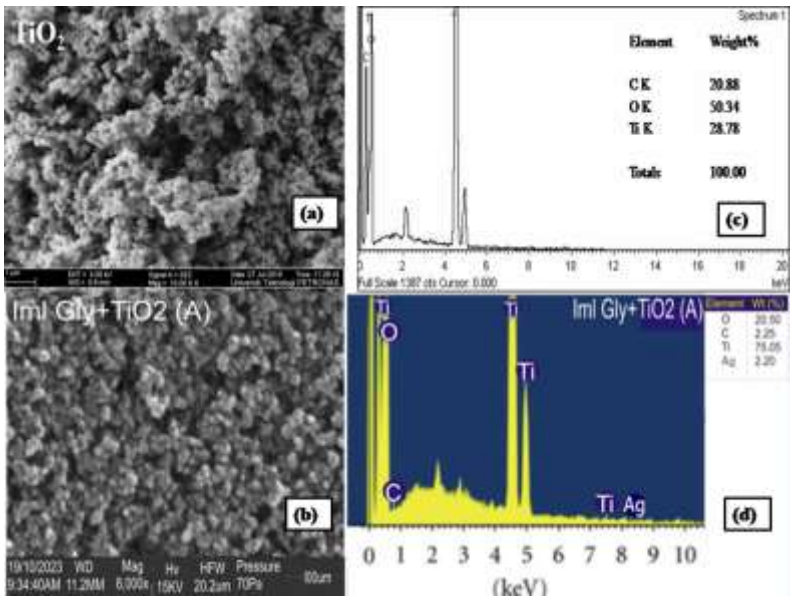

Figure 9: (a) SEM micrograph of TiO_2, (b) SEM micrograph of TiO_2 incorporated with the synthesized AgNPs, and (c) EDS result of the TiO_2 nanoparticles (d) EDS result for the TiO_2 nanocomposite

TEM characterizations of the AgNPs, TiO_2, and TiO_2 nanocomposite were also performed to augment the structural characterizations. The sizes of the particles in the TEM micrographs and their distributions were calculated using imageJ software [version 1.42q (2483 x 1900 nm magnification), National Institute of Health, USA] and Origin 2021 software. Figure 10 (a) shows the TEM image of the AgNPs which clearly indicate that the AgNPs are spherical in form. The size distribution histogram in Figure 10 (b) indicates that the TEM micrograph also validates the creation of AgNPs with an average size of 4.14 nm.

Figure 11 shows the TEM images of the TiO_2 film and TiO_2 film integrated with the AgNPs. According to the TEM image in Figure 11(a), the TiO_2 has a broad size variation between 2 and 22 nm and is spherical in shape. As demonstrated by the size distribution histogram in Figure 11(c), the TEM micrograph also validates the creation of particles with an average size of 7.98 nm.

Figure 11 (b) shows the TEM image of the TiO_2 integrated with the AgNPs. According to the image, the nanoparticle is spherical in shape and has a broad size distribution between 2 and 12 nm, with a significant proportion of the particles falling between 3 and 8 nm. Additionally, it validates the development of nanoparticles with an average size of 5.39 nm, as demonstrated by the size distribution histogram in Figure 11(d).

It has been observed that a greater surface area is necessary to enhance the light absorption of TiO_2, and that the surface area is related to the nanoparticle size [13]. A nanoparticle's surface area increases with decreasing particle size, increasing the likelihood of collisions and speeding up the rate of reaction [14]. The behaviors Ag/TiO_2 nanocomposites is significantly affected by particle size reduction since it alters surface area, dispersion, electrical characteristics, and catalytic performance, all of which can be used to improve the particles' usefulness in DSSC applications [31].

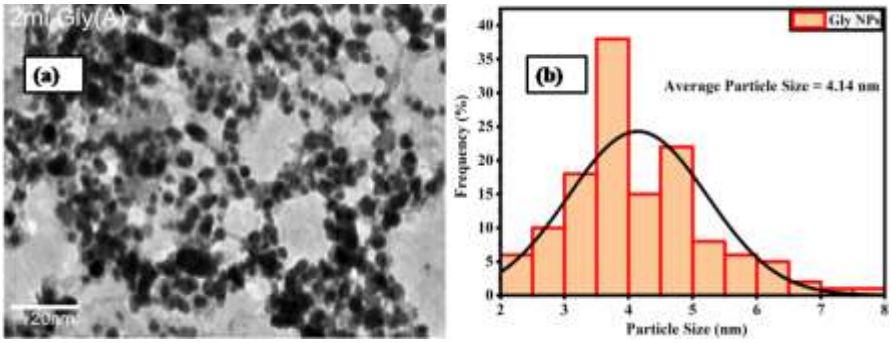

Figure 10: (a) TEM image of the AgNPs (b) Corresponding size distribution histogram

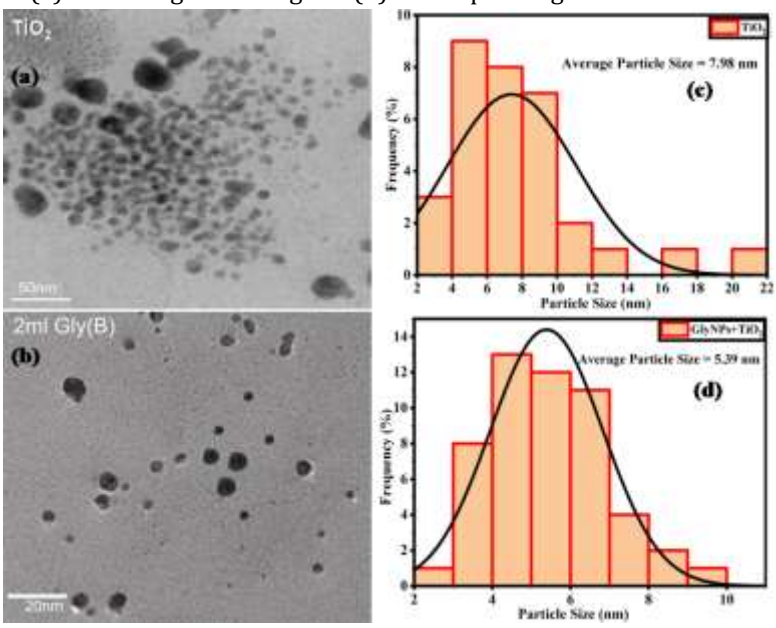

Figure 11: (a) TEM image of TiO_2 alone, (b) TEM image of TiO_2 incorporated with the AgNPs, (c) Corresponding size distribution histogram of TiO_2, and (d) Corresponding size distribution histogram of TiO_2 incorporated with the AgNPs

Electrical characterizations Ag/TiO_2 thin films

The electrical characteristics of the TiO_2 film and the modified TiO_2 film were examined using a four-point probe. The method was applied to determine the samples' conductivity, resistivity, and resistance [32]. The films' cross-sectional area was 9.75 cm^2, and their length between the probes was 6.5 cm. The resistivity (ρ) was calculated in terms of open circuit voltage (V_{oc}) and short circuit current (I_{sc}) using Equation (1), while the resistance (R) was estimated by Equation (2). Conductivity (σ) was given as the reciprocal of resistivity [32].

$$\rho = \frac{\pi}{ln2} \cdot \frac{V_{oc}}{I_{sc}} \quad (1)$$

$$R = \frac{\rho L}{A} \quad (2)$$

The voltage and current density graphs for the TiO_2 film and the modified TiO_2 film are displayed in Figure 12. Additionally, Table 4 contains a summary of the electrical parameters for film and modified film. It was evident that the TiO_2 film had a voltage (V) of 0.53 V and a current (I) of 1.81 µA. The TiO_2 film containing the AgNPs had a voltage of 0.61 V and a current of 2.85 µA. It was clear that the addition of AgNPs to the film significantly reduced the calculated resistance and resistivity. Consequently, the inclusion of AgNPs enhanced the conductivity by 73.11%, which in turn improved the electrical properties and increased electron mobility [32,33].

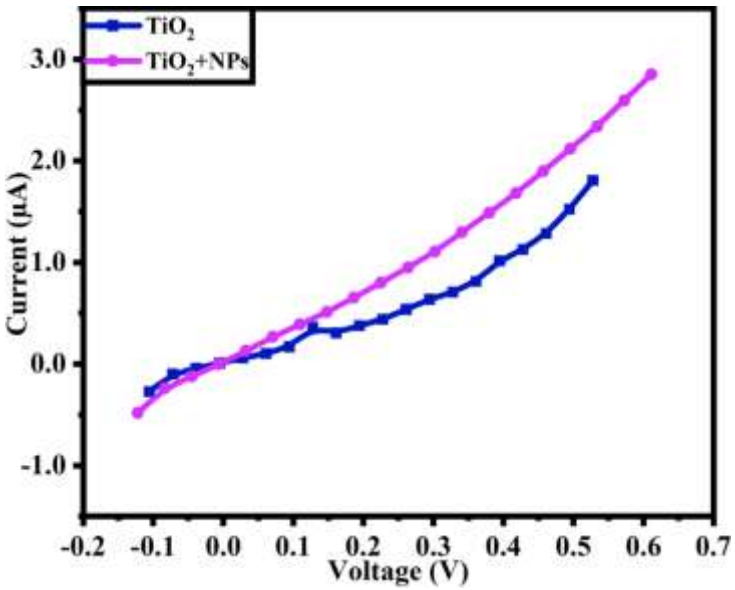

Figure 12: Graphs of current versus voltage for TiO_2 and modified TiO_2 films

Table 4: Summary of the electrical characteristics of TiO_2 and modified TiO_2 films

Sample	TiO_2 film	TiO_2 film with AgNPs
Length Between Probes (cm)	6.5	6.5
Area of Thin Film (cm^2)	9.75	9.75
Current, (μA)	1.81	2.85
Voltage, (V)	0.53	0.61
Resistance, R (Ω)	8.85×10^5	6.47×10^5
Resistivity, ρ (Ωm)	13.27×10^5	9.70×10^5
Conductivity, σ (S/m)	7.53×10^{-7}	1.03×10^{-6}

The addition of AgNPs to TiO_2 film causes the individual particles to become linked, facilitating free electron movement and raising the overall conductivity. Conductivity significantly increases as a result of the formation of a continuous conductive channel. AgNPs also exhibit SPR, which contributes to their enhanced conductivity. An electrical signal is magnified when light strikes the film's surface because the electromagnetic waves stimulate the free electrons of the silver particles. This effect improves the conductivity, increasing the films' ability to transfer electrical signals effectively. Moreover, silver particles create a solid link with the TiO_2 surface as they integrate into the layer. A greater conductivity is the outcome of this bonding's enhanced ability to transport electrical charges [32,33]. The conductivity was also improved by the two materials' creation of a contact between silver, oxygen, and titanium in the two materials. The conductivity was also significantly influenced by the insulating amorphous carbon layer that developed just around the AgNPs.

By preventing direct contact between the Ag particles and the insulating matrix, it allowed electrons to flow freely and helped stabilize the thin layer. The increase in conductivity is mostly observed in the film's bulk conduction, which means it permeates the entire material rather than just the surface.

This is significant because it implies that rather than depending on a surface layer to carry the current, the film as a whole may efficiently conduct electricity [32,33]

Conclusion

The development and characterization of a green-synthesized Ag/TiO_2 nanocomposite, as well as its usage as an enhanced photoanode material in DSSCs, were demonstrated by this study using *G. sepium* leaf extract. The absorbance spectral analysis revealed that the absorbance was improved with the AgNPs' inclusion into TiO_2. As the absorbance increased, the energy gap decreased. The detected functional groups and their possible contribution to the nanoparticle's formation were revealed by the FTIR study results. The AgNPs and the nanocomposite were also found to be crystalline in nature, with average crystallite sizes of 3.69 nm and 4.04 nm, respectively, according to XRD results. The morphology of the AgNPs verified that they were uniformly distributed, well-formed and spherical. When coupled with the nanoparticle, the TiO_2's surface became smoother and more spherical in shape. EDS of the TiO_2 nanoparticle and TiO_2 nanocomposite confirmed the presence of Ag and other chemical components. The creation of AgNPs and nanocomposite with average sizes of 4.14 nm and 5.39 nm, respectively, was further confirmed by the evaluation of the particles' TEM micrographs. The electrical properties for films and modified films showed that the calculated resistance and resistivity significantly decreased when the films were incorporated with AgNPs. As a result, the addition of AgNPs increased the conductivity by 73.11%, which enhanced electron mobility and electrical properties. The improved conductivity of the TiO_2 films combined with the AgNPs and the interaction between TiO_2 and Ag had demonstrated promising characteristics and may be suggested for application in DSSCs.

Acknowledgments

O. A. acknowledges the assistance from the TETFUND 2024 Institution Based Research (IBR) fund LAUTECH, Nigeria. Furthermore, the authors acknowledge the Department of Pure and Applied Physics at LAUTECH, Nigeria, for the UV-Vis analysis, and the Engineering Materials and Development Institute at Ondo State University in Akure, Nigeria, for the thin film analyses and IV characterizations

ORCID

Joseph Adegbite Adebanji: 0009-0004-7332-9322
Gabriel Ayinde Alamu: 0000-0003-2783-8738
Olufunke Lydia Adedeji: 0000-0002-5982-8983
Khadijat Kuburat Babalola: 0009-0001-1982-6043
Ayodele Joshua Abiodun: 0000-0002-6596-2505
Hakeem Olayinka Oyeshola: 0000-0002-1628-1455
Oluwaseun Adedokun: 0000-0002-7947-8415
Yekinni Kolawole Sanusi: 0000-0001-6259-1166

Reference

[1] Alamu, G.A., Adedokun, O., Bello, I.T., Sanusi, Y.K., Plasmonic enhancement of visible light absorption in Ag-TiO_2 based dye-sensitized solar cells. *Chemical Physics Impact*, **2021**, 3, 100037.
[2] Jubu, P., Mbakaan, C., Adedokun, O., Danladi, E., Kyesmen, P., Nathan-Abutu, A., Barakur, C., Igba, V., Pakhuruddin, M., Yam, F., Facile fabrication of TiO_2-TiN nanocomposite by one-batch thermal oxidation and ammonolysis technique: Structural, optical and photoelectrocatalytic properties. *Materials Science and Engineering: B*, **2025**, 313, 117952.
[3] Sasikumar, R., Thirumalaisamy, S., Kim, B., Hwang, B., Dye-sensitized solar cells: Insights and research divergence towards alternatives. *Renewable and Sustainable Energy Reviews*, **2024**, 199, 114549.
[4] Adedokun, O., Muraina, A.O., Jubu, P.R., Oyewole, O.J., Zaki, Z.I., Khalifa, M.E., Vyas, S., Obaseki, O.S., Yam, F.K., Synergistic enhancement of photoelectrochemical water splitting by Ag and Zn nanoparticle-decorated TiO_2 nanorods. *Journal of Materials Science: Materials in Electronics*, **2025**, 36(11), 644.
[5] Hirbodi, S., Jamekhorshid, A., Jalali, T., Mohammadian, J., Osfouri, S., Enhanced efficiency, electron lifetime, and eco-friendliness of dye-sensitized solar cells using nanofibrous TiO_2/ZnO composite photoanodes and natural anthocyanin sensitizer. *Results in Surfaces and Interfaces*, **2024**, 17, 100339.
[6] Ahmad, M.S., Pandey, A.K., Abd Rahim, N., Advancements in the development of TiO_2

photoanodes and its fabrication methods for dye sensitized solar cell (DSSC) applications. A review. *Renewable and Sustainable Energy Reviews*, **2017**, 77, 89–108.
[7] Srivastava, K.V., Srivastava, P., Srivastava, A., Maurya, R.K., Singh, Y.P., Srivastava, A., 1D TiO_2 photoanodes: A game-changer for high-efficiency dye-sensitized solar cells. *RSC Advances*, **2025**, 15(7), 4789–4819.
[8] Benhaliliba, M. Opto-Electrical Characterization of SnO2 Semiconductor Based Thin Layer for the Fabrication of Innovative Diode. *Journal of Engineering in Industrial Research*, **2025**, 6(1), 1-18.
[9] Sharma, K., Sharma, V., Sharma, S., Dye-sensitized solar cells: Fundamentals and current status. *Nanoscale Research Letters*, **2018**, 13(1), 381.
[10] Lana, G.M., Bello, I.T., Adedokun, O.M., Adenigba, V.O., Jubu, P.R., Adedokun, O., Sanusi, Y.K., Dhlamini, M.S., Awodugba, A.O., One-dimensional TiO_2 nanocomposite-based photoanode for dye-sensitized solar cells: A review. *Solar Energy*, **2024**, 279, 112850.
[11] Muhammad, A., Riffat, Y., Rizwan, A., Ana, A., Madihaand, M., Shehla, U. Green Synthesis of Silver Nanoparticles (AgNPs), Structural Characterization and their Antibacterial Potentials. *National Centre for Biotechnology Information*, **2022**, 20(2) 15593258221088709.
[12] Verma, A., Mehata, M.S., Controllable synthesis of silver nanoparticles using neem leaves and their antimicrobial activity. *Journal of Radiation Research and applied sciences*, **2016**, 9(1), 109–115.
[13] Raut, R., Lakkakula, J., Kolekar, N., Sahebrao, K., Phytosynthesis of Silver Nanoparticle using Gliricidia sepium (Jacq.). *Current Nanoscience*, **2009**, 5(1), 12-117.
[14] Devatha, C., Jagadeesh, K., Patil, M., Effect of green synthesized iron nanoparticles by azardirachta indica in different proportions on antibacterial activity. *Environmental Nanotechnology, Monitoring & Management*, **2018**, 9, 85–94.
[15] Ren, Y.-y., Yang, H., Wang, T., Wang, C., Bio-synthesis of silver nanoparticles with antibacterial activity. *Materials Chemistry and Physics*, **2019**, 235, 121746.
[16] Hwang, H.-J., Joo, S.-J., Patil, S.A., Kim, H.-S., Efficiency enhancement in dye-sensitized solar cells using the shape/size-dependent plasmonic nanocomposite photoanodes incorporating silver nanoplates. *Nanoscale*, **2017**, 9(23), 7960–7969.
[17] Adedokun, O., Awodele, M. K., Sanusi, Y. K., Awodugba, A. O. Natural Dye Extracts from Fruit Peels as Sensitizers in ZNO-Based Dye-Sensitized Solar Cells. *IOP Conference Series: Earth and Environmental Science.,* 2018, 173, 012040.
[18] Kiruba Daniel, S., Vinothini, G., Subramanian, N., Nehru, K., Sivakumar, M., Biosynthesis of Cu, ZVI, and Ag nanoparticles using dodonaea viscosa extract for antibacterial activity against human pathogens. *Journal of Nanoparticle Research*, **2013**, 15(1), 1319.
[19] Obaid, A.Y., Al-Thabaiti, S.A., El-Mossalamy, E., Al-Harbi, L.M., Khan, Z., Extracellular bio-synthesis of silver nanoparticles. *Arabian Journal of Chemistry*, **2017**, 10(2), 226–231.
[20] Ito, S., Murakami, T.N., Comte, P., Liska, P., Grätzel, C., Nazeeruddin, M.K., Grätzel, M., Fabrication of thin film dye sensitized solar cells with solar to electric power conversion efficiency over 10%. *Thin Solid Films*, **2008**, 516(14), 4613–4619.
[21Levchuk, I., Sillanpää, M., Guillard, C., Gregori, D., Chateau, D., Chaput, F., Lerouge, F., Parola, S., Enhanced photocatalytic activity through insertion of plasmonic nanostructures into porous TiO_2/SiO_2 hybrid composite films. *Journal of Catalysis*, **2016**, 342, 117–124.
[22] Kumar, K.M., Mandal, B.K., Sinha, M., Krishnakumar, V., Terminalia chebula mediated green and rapid synthesis of gold nanoparticles. *Spectrochimica Acta Part A: Molecular and Biomolecular Spectroscopy*, **2012**, 86, 490–494.
[23] Zayed, M.F., Eisa, W.H., Shabaka, A., Malva parviflora extract assisted green synthesis of silver nanoparticles. *Spectrochimica Acta Part A: Molecular and Biomolecular Spectroscopy*, **2012**, 98, 423–428.
[24] Yew, Y.P., Shameli, K., Miyake, M., Kuwano, N., Bt Ahmad Khairudin, N.B., Bt Mohamad, S.E., Lee, K.X., Green synthesis of magnetite (Fe_3O_4) nanoparticles using seaweed (kappaphycus alvarezii) extract. *Nanoscale Research Letters*, **2016**, 11(1), 276.
[25] Kim, I. H., Park, E. J., Park, C. H., Han, S. H., Seo, H. O., Kim, Y. D. Green synthesis of iron oxide nanoparticles using *Platanus orientalis* leaf extract for antifungal activity, *Catalysis Today,* **2017**, 295, 54–64
[26] Babu, M.G., Gunasekaran, P., Production and structural characterization of crystalline silver nanoparticles from bacillus cereus isolate. *Colloids and Surfaces B: Biointerfaces*, **2009**, 74(1), 191–195.
[27] Shukla, S., Jadaun, A., Arora, V., Sinha, R.K., Biyani, N., Jain, V., In vitro toxicity assessment of chitosan oligosaccharide coated iron oxide nanoparticles. *Toxicology Reports*, **2015**, 2, 27–39.
[28] Chang, Y.-C., Chen, D.-H., Preparation and adsorption properties of monodisperse chitosan-bound Fe_3O_4 magnetic nanoparticles for removal of cu(II) ions. *Journal of Colloid and Interface Science*, **2005**, 283(2), 446–451.
[29] Basavegowda, N., Idhayadhulla, A., Lee, Y.R., Preparation of Au and Ag nanoparticles using artemisia annua and there in vitro antibacterial and tyrosinase inhibitory activities. *Materials Science and*

Engineering: C, **2014**, 43, 58–64.
[30] Zhang, J., Ahmadi, M., Fargas, G., Perinka, N., Reguera, J., Lanceros-Méndez, S., Llanes, L., Jiménez-Piqué, E., Silver nanoparticles for conductive inks: From synthesis and ink formulation to their use in printing technologies. *Metals*, **2022**, 12(2), 234.
[31] Sarkar, P., Panda, S., Maji, B., Mukhopadhyay, A. K. Comparative Study of Au and Ag Nanoparticle to Improve in Absorption in Plasmonic Solar Cell. *Devices for Integrated Circuit (DevIC)*, **2017**, 175-179.
[32] Khan, M., Bhatti, K., Qindeel, R., Bousiakou, L.G., Alonizan, N., Investigations of the structural, morphological and electrical properties of multilayer ZnO/TiO_2 thin films, deposited by sol–gel technique. *Results in Physics*, **2016**, 6, 156–160.
[33] Khodayari, M.M., Rouhi, S., Design and fabrication of nano solar cell on ultra-light silica substrate, *Asian Journal of Green Chemistry*, **2025**, 9(1): 101-114.